

The variational approximation for two-dimensional quantum droplets

Sherzod R. Otajonov, Eduard N. Tsoy, and Fatkhulla Kh. Abdullaev
*Physical-Technical Institute of the Uzbek Academy of Sciences,
 Chingiz Aytmatov str. 2-B, Tashkent, 100084, Uzbekistan*
 (Dated: December 25, 2020)

The dynamics of a two-dimensional Bose-Einstein condensate in a presence of quantum fluctuations is studied. The properties of localized density distributions, quantum droplets (QDs), are analyzed by means of the variational approach. It is demonstrated that the super-Gaussian function gives a good approximation for profiles of fundamental QDs and droplets with non-zero vorticity. The dynamical equations for parameters of QDs are obtained. Fixed points of these equations determine the parameters of stationary QDs. The period of small oscillations of QDs near the stationary state is estimated. It is obtained that periodic modulations of the strength of quantum fluctuations can actuate different processes, including resonance oscillations of the QD parameters, an emission of waves and a splitting of QDs into smaller droplets.

Keywords: Quantum droplets; Bose-Einstein condensate; two-dimensional solitons; quantum fluctuations

I. INTRODUCTION

The quantum pressure and the two-body interaction (2BI) are the basic effects that determine the mean-field dynamics of Bose-Einstein condensates (BECs) [1]. A balance between these two effects can result in a formation of matter-wave solitons. Solitons are stable in one-dimensional (1D) systems with attractive cubic non-linearity, but they are unstable in higher dimensions. Different methods are suggested to stabilize localized waves in 2D and 3D BECs. These methods include an account of higher-order nonlinearities, an application of external traps, an account of the dipolar interaction, and a dynamical variation of the interaction parameter [1, 2].

Recently, it was suggested that quantum fluctuations (QFs) can stabilize localized waves in BECs [3, 4]. Moreover, it was shown that QFs are responsible for a formation of quantum droplets (QDs), which are clusters of an ultra-dilute liquid. Quantum fluctuations are effects beyond the mean-field description of BECs. These effects are described by the Lee-Huang-Yang (LHY) correction term [5] in the BEC Hamiltonian. Usually, the influence of QFs is small comparing with the 2BI. A decrease of the 2BI parameter via the Feshbach resonance does not help to reveal QFs, since the parameter of the LHY term diminishes as well. However, in BEC mixtures, it is possible to tune the parameters of intra-species and inter-species interactions in such a way that the residual 2BI is comparable with QFs [3, 4]. Indeed, a formation of QDs in binary BECs was observed experimentally [6, 7].

A dipolar BEC is another example of atomic systems, where the effect of QFs can be made pronounced. The strength of the dipolar interaction can be tuned independently of the LHY parameter. Then, the dipolar interaction can almost balance the 2BI, making QFs appreciable. An ultra-dilute liquid and QDs were also observed experimentally in dipolar BECs [8].

In the present paper, we study QDs in a binary 2D BEC. Basically, QDs are solitons induced by quantum fluctuations. We consider such a situation, when the dy-

namics of the BEC components is described by a single equation. This situation is possible in the symmetric case, when the component densities, as well as the coupling constants, are close to each other, see Ref. [4] and Sec. II A. Such a condition was used in other studies [4, 9, 10] as well. We apply the variational approximation (VA), and demonstrate that the super-Gaussian function describes well QDs in a wide range of the system parameters. We obtain explicit relations that define stationary and dynamical parameters of two-dimensional QDs. A response of QDs to the periodic modulation in time of the LHY parameter is analyzed as well.

II. RESULTS

A. The model and the variational approximation

We consider a binary 2D BEC with the repulsive intra-species interaction and attractive inter-species interaction. The dynamics of the BEC in a presence of quantum fluctuations is governed by the following equations [4]

$$i\hbar \frac{\partial \phi_j}{\partial T} = -\frac{\hbar^2}{2m} \nabla^2 \phi_j + \left[(-1)^{j-1} g_j^{1/2} \times \right. \\ \left. (g_1^{1/2} |\phi_1|^2 - g_2^{1/2} |\phi_2|^2) + \frac{g_j P}{4\pi\eta} \log \frac{Pe}{\eta\Delta} \right] \phi_j, \quad (1)$$

where ϕ_j are the component wave functions, $\nabla^2 = \partial_X^2 + \partial_Y^2$, T is time, $g_j = \frac{4\pi\eta}{\log[4e^{-2C}/(a_j^2\Delta)]}$ are the modified coupling constants, $P = g_1 |\phi_1|^2 + g_2 |\phi_2|^2$, $\Delta = \frac{4e^{-2C}}{|a_x| \sqrt{a_1 a_2}} \exp\left\{ \frac{-\log^2(a_2/a_1)}{2 \log[a_x^2/(a_1 a_2)]} \right\}$, $\eta = \hbar^2/m_a$, $j = 1$ and 2 , m_a is the atom mass, a_1 and a_2 (a_x) are the 2D intra-species (inter-species) scattering lengths [4], and $C \approx 0.5772$ is the Euler constant.

In the symmetric case, $\phi_1 = \phi_2 = \phi$ and $g_1 = g_2 = g$, Eqs. (1) are reduced to the single Gross-Pitaevskii equation [4, 9] in the dimensionless form

$$i\partial_t \Psi + \frac{1}{2} \nabla^2 \Psi + \gamma |\Psi|^2 \Psi + \delta |\Psi|^2 \log(|\Psi|^2) \Psi = 0, \quad (2)$$

where $\Psi = \phi/\sqrt{n_0}$, $\nabla^2 = \partial_y^2 + \partial_x^2$, $x = X/X_{sc}$, $y = Y/Y_{sc}$, $t = T/T_{sc}$, $\delta = -g^2 n_0 m / (\pi \hbar^3 \omega_0)$ characterizes the strength of QFs, $\gamma = -\delta/2$, and $n_0 = \Delta / (2ge^{3/2})$ is the equilibrium density of a component [4]. The time scale and the spatial scale are defined in Eq. (2) as $T_{sc} = \omega_0^{-1}$, and $X_{sc} = Y_{sc} = [\hbar / (m\omega_0)]^{1/2}$, respectively, where ω_0 is the characteristic frequency of the external trapping potential [1]. When $\gamma > 0$ and $\delta = 0$, there are no stable localized solutions in the system. For these values, solitons either decay or collapse, depending on initial conditions [11]. Quantum fluctuations, described by the LHY term with $\delta < 0$, arrest the collapse [3, 4].

There are certain indications that the symmetric state is stable. A deviation from the symmetric state adds a non-negative term to the energy [4]. Also, numerical simulations for the non-symmetric case in Ref. [9] show results consistent with the symmetric case. Below, we assume that small perturbations of the symmetric state do not change substantially the dynamics.

The Lagrangian density of Eq. (2) is defined as follows

$$\mathcal{L} = \frac{i}{2}(\Psi^* \partial_t \Psi - \Psi \partial_t \Psi^*) - \frac{1}{2}(|\partial_x \Psi|^2 + |\partial_y \Psi|^2) + \frac{\gamma}{2}|\Psi|^4 + \frac{\delta}{2}|\Psi|^4 \log\left(\frac{|\Psi|^2}{\sqrt{e}}\right). \quad (3)$$

By using transformation $\Psi \exp[\gamma/(2\delta)] \rightarrow \bar{\Psi}$ and $\delta \exp(-\gamma/\delta) \rightarrow \bar{\delta}$, we can eliminate terms proportional to γ in Eqs. (2) and (3), even when γ and δ are independent. Therefore, below we take $\gamma = 0$, however, results obtained are valid also for the general case. The energy density \mathcal{E} of a BEC is related to \mathcal{L} as

$$\mathcal{E} = \frac{i}{2}(\Psi^* \partial_t \Psi - \Psi \partial_t \Psi^*) - \mathcal{L}. \quad (4)$$

Function $V(x, t) \equiv -\delta|\Psi|^2 \log|\Psi|^2$ in the last term of Eq. (2) can be considered as an effective self-induced potential for field Ψ . When $\delta < 0$, a pulse-shaped distribution of the BEC density with $|\Psi|^2 < 1$ results in an attractive potential $V(x, t)$. This attractive force due to quantum fluctuations can balance the quantum pressure, described by the second term in Eq. (2), so that a formation of localized waves (vortices) is possible.

There are no known solutions of Eq. (2). In order to characterize QDs, we employ the following super-Gaussian trial function:

$$\Psi(r, \theta, t) = Ar^S \exp\left[-\frac{1}{2}\left(\frac{r}{w}\right)^{2m} + i(br^2 \pm S\theta + \varphi)\right], \quad (5)$$

where $A(t)$, $w(t)$, $b(t)$, and $\varphi(t)$ are the variational parameters, denoting the amplitude parameter, width, chirp, and the initial phase, respectively. Parameter m defines the profile shape. When $m \approx 1$ and $S = 0$, the profile has a bell shape, while when $m \gg 1$ ($0 < m \ll 1$), the profile tends to a flat-top (cusp) shape. The non-negative integer parameter $S \geq 0$ is the topological charge (vorticity) of a QD. The fundamental (zero-vorticity) QD has $S = 0$, while vortex QDs have $S > 0$.

The plus (minus) sign in a front of S corresponds to a vortex (anti-vortex). Parameter A is related to the maximum \bar{A}^2 of the QD density as the following

$$\bar{A} = A(MS)^{MS/2} w^S \exp(-MS/2), \quad (6)$$

where $M = 1/m$. When $S = 0$, the QD size is specified by parameter w , such that the full width at half maximum, w_{FWHM} is found as $w_{FWHM} = 2(\log 2)^{M/2} w$. When $S > 0$, the QD size can be defined as a position of the density maximum, $r_{max} = (MS)^{M/2} w$.

When $A(t) = \text{const}$ and $w(t) = \text{const}$, Eq. (5) gives an approximation of a stationary solution $\Psi(r, \theta, t) = u(r, \theta) \exp(-i\mu t)$ of Eq. (2), where $u(r, \theta)$ is a profile function, and μ is the chemical potential, see Eq. (15). We mention that the super-Gaussian function describes well (with accuracy 1-5%) 1D quantum droplets [12]. As it is shown below, this function gives also a reasonable approximation for profiles and parameters of 2D QDs.

Norm N is the conserved quantity of Eq. (2), and it is proportional to the number of atoms in a BEC cloud. In terms of the trial function, N is written as

$$N = \iint_{-\infty}^{\infty} |\Psi|^2 dx dy = \pi M A^2 w^{2(S+1)} \Gamma(M(S+1)). \quad (7)$$

Substituting the trial function into Eq. (3), and integrating over the spatial variable, we get the averaged Lagrangian $L = \iint \mathcal{L} dx dy$

$$\frac{L}{N} = -\varphi' - \frac{\Gamma(M(S+2))}{\Gamma(M(S+1))} w^2 (2b^2 + b') - G, \quad (8)$$

where the prime denotes the time derivative, and

$$G(w, N, M) = \frac{\Gamma(MS+2)}{2M^2 \Gamma(M(S+1)) w^2} + \frac{N \Gamma(M(2S+1))}{2^{2+M(2S+1)} \pi M \Gamma^2(M(S+1)) w^2} \times \delta \left\{ 1 + M + 2MS [1 - \psi(M(2S+1))] - 2 \log \left[\frac{N}{2^{MS} \pi M w^2 \Gamma(M(S+1))} \right] \right\}. \quad (9)$$

Here $\Gamma(z)$ is the Gamma function, and $\psi(z) = d \ln \Gamma(z) / dz$ is the digamma function. The Euler-Lagrangian equations for L result in the following set of equations for the QD parameters:

$$\begin{aligned} b' &= -2b^2 - \frac{\Gamma(M(S+1))}{2\Gamma(M(S+2))} \frac{1}{w} \frac{\partial G}{\partial w} \equiv f_b, \\ w' &= 2bw \equiv f_w, \\ f_m &\equiv \frac{\partial L}{\partial m} = 0. \end{aligned} \quad (10)$$

The parameters of a stationary QD are found from $b = 0$, $f_b(w, N, m) = 0$, and $f_m(w, N, m) = 0$. Therefore, similarly to Ref. [12], we state that for a given set of the

system parameters, index m takes the value that corresponds to a stationary state.

The first two equations of Eqs. (10) can further be combined into a single equation for the QD width:

$$w'' = -\frac{\Gamma(M(S+1))}{\Gamma(M(S+2))} \frac{\partial G}{\partial w} \equiv -\frac{\partial U(w)}{\partial w}. \quad (11)$$

Therefore, the dynamics of the QD parameters is reduced to the dynamics of an effective particle with coordinate w in a potential $U(w)$, see also Ref. [12]:

$$U(w) = \frac{\Gamma(M(S+1))}{\Gamma(M(S+2))} G. \quad (12)$$

The potentials for different values of (S, N, m) are plotted in Fig. 1. The minimum of the potential [or a zero of $f_b(w, N, m) = 0$] corresponds to width w_s of a stationary quantum droplet:

$$w_s = \frac{\sqrt{N}}{\sqrt{2^{MS} \pi M \Gamma(M(S+1))}} e^c, \quad (13)$$

where

$$c = \frac{1}{4} \left[1 - M(2S+1) + 2MS\psi(M(2S+1)) - 2^{1+M(2S+1)} \frac{\pi \Gamma(MS+2) \Gamma(M(S+1))}{\delta M N \Gamma(M(2S+1))} \right]. \quad (14)$$

For given S and N , the width w_s depends only on m , which is determined from $f_m(w_s, N, m) = 0$. Then, the amplitude parameter A_s of a stationary droplet is obtained from Eq. (7), while the chemical potential $\mu \equiv -\varphi'$ is found as

$$\mu = \left. \frac{\partial E_s}{\partial N} \right|_{w=w_s} = \left. \frac{\partial (NG)}{\partial N} \right|_{w=w_s}. \quad (15)$$

where $E_s = \iint \mathcal{E} dx dy = NG$ is the energy of the stationary QD. Thus, the VA provides equations for calculation of main parameters of stationary QDs. The inset of Fig. 1 shows the dependencies of the chemical potential μ on norm N for the values of $S = 0, 1$, and 2. The chemical potential approaches a constant value at large N . This is typical for flat-top solitons. For a reference, the Thomas-Fermi limit $\mu_{\text{TF}} = -1/(2\sqrt{e})$ [9], valid for large N , is also shown in the inset of Fig. 1. Analysis of other parameters of stationary QDs are presented in Sec. II B. We provide also approximate equations for m so that the QD parameters can be calculated directly.

The frequency of small oscillations near the stationary width is obtained by using Eq. (12)

$$\Omega_0^2 = \left. \frac{\partial^2 U(w)}{\partial w^2} \right|_{w=w_s} = \frac{\Gamma(M(S+1))}{\Gamma(M(S+2))} \left. \frac{\partial^2 G}{\partial w^2} \right|_{w=w_s}. \quad (16)$$

The frequency Ω_0 defines the frequency of the Goldstone mode of a QD, oscillating near the stationary state. This

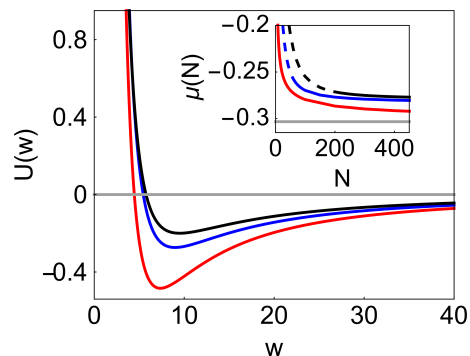


FIG. 1. (color online) The shape of effective potentials for different parameters of (S, N, m) . The bottom (red), middle (blue) and top (black) lines are for $(0, 100, 2.537)$, $(1, 200, 1.971)$, and $(2, 200, 2.073)$, respectively. The inset shows the chemical potential μ as a function of norm N , see Eq. (15). The order (color) and parameters of the curves are the same as in the main plot. Dashed lines for $S = 1$ and 2 correspond to numerically unstable regions. The gray line in the inset represents the Thomas-Fermi limit.

parameter can be used in experiments to estimate the strength of QFs.

Quantum fluctuations are described by the LHY term with $\delta < 0$, however the VA allows us to analyze the opposite case as well. When $\delta > 0$, the potential $U(w)$ tends to $-\infty$ at $w \rightarrow 0$, to 0 at $w \rightarrow \infty$, and has a single maximum at $w = w_s$, which corresponds to an unstable stationary solution. This value is small, $w_s \lesssim 0.5$ for $\delta = 1$ and $N = [1, 1000]$. Moreover, for $S = 0$ and $N \gtrsim 6.3$ the value of μ becomes positive, and $m < 0.5$. Value w_s is a threshold that separates different types of the dynamics. For given N , if the initial width is larger (smaller) than the threshold, then the soliton decays dispersively (collapses). In numerical simulations, the threshold value is $\sim (1.05-1.1) w_s$. A presence of a collapse has a simple physical explanation. When $\delta > 0$ and $|\Psi|^2 > 1$, the last term in Eq. (2) corresponds to self-attraction. Since the order of nonlinearity is greater than cubic, the attraction cannot be balanced by dispersion, resulting in a collapse in the system.

B. Numerical simulations

A comparison of the stationary QD parameters, found from the VA, with those, found from numerical simulations of Eq. (2), is presented in Fig. 2. In numerical simulations of Eq. (2), we take an initial condition in form (5) with parameters A_s , w_s , and m_s , found from the VA. Then Eq. (2) is integrated by the split-step Fourier (SSF) method with 512×512 discrete points and the spatial region of size $d \times d$, where $d \sim 50-100$, depending on the QD width. Absorbing boundary conditions are used to prevent reflections of waves, emitted by a QD, from the end points of the region.

An exact stationary solution has a time-independent spatial distribution of the BEC density. However, we observe small oscillations on time of the QD parameters near a stationary state. The relative amplitude of oscillations is less than few percent of the stationary value that shows an acceptable accuracy of the VA. An additional change of the initial parameters by $\sim 1\text{--}5\%$ results just in a corresponding small increase of the amplitude of oscillations, indicating the stability of the stationary state. The amplitude parameter A is found from the maximum \bar{A}^2 of the field density and Eq. (6). The QD width is found numerically from the following equation

$$w^2 = \frac{\Gamma(M(S+1))}{\Gamma(M(S+2))N} \iint_{-\infty}^{\infty} (x^2 + y^2) |\Psi|^2 dx dy. \quad (17)$$

We mention that this equation gives acceptable values of the width when deviations from the stationary profile are small. Stationary values of the QD parameters are found as an average on time after several initial oscillations. Figure 2 demonstrates that the VA gives a good prediction, and that the super-Gaussian profile is close to the actual stationary solution of Eq. (2). The behavior described above is valid for sufficiently large N . For smaller N , stationary states can be unstable (see below).

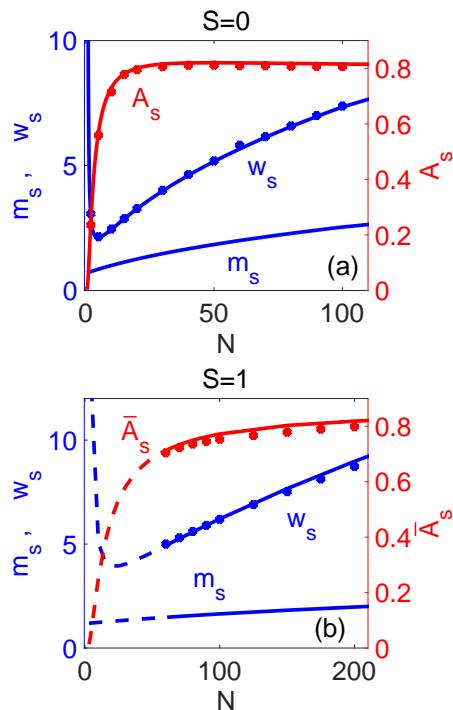


FIG. 2. (color online) (a) Parameters of stationary QDs, found from the VA (lines) and from numerical simulations (points) of Eq. (2) for $S = 0$. The left axis is for QD width w_s and m_s , while the right axis is for parameter A_s . (b) The same as in panel (a) but for $S = 1$. Dashed lines correspond to numerically unstable regions.

It follows from Fig. 2 that the QD amplitude A_s tends

to a constant value for large N , while the width increases on N . This fact and a gradual increase of m_s mean that a QD approaches the flat-top shape for large N . For practical purpose, we approximate dependence $m_s(N)$ for $\delta = -1$ as

$$\begin{aligned} m_s &= (0.4433 + 0.05906N)^{0.5047} & \text{for } S = 0, \\ m_s &= (1.519 + 0.02415N)^{0.3692} & \text{for } S = 1. \end{aligned} \quad (18)$$

A functional form of $m_s(N) = (a_1 + a_2N)^k$ is taken empirically, and parameters are found by fitting with values of m_s , found numerically from the VA for $0 < N \leq 1000$. Using Eqs. (18), we can find directly the stationary width w_s from Eq. (13), then A_s from Eq. (7), and μ from Eq. (15).

In Fig. 3, we present a comparison of stationary QD profiles, found from the VA, with those, found from the imaginary-time method. For $S = 0$, the profiles, obtained by the two methods, are very close to each other in a wide range of N . For $S = 0$, we choose $N = 1000$ in order to demonstrate a flat-top shape of QDs. We take $N = 60, 200$ and 510 for vortices with $S = 1, 2$ and 3 , respectively. We mention that the norm values chosen for $S > 0$ correspond to the stability thresholds (see below). Figure 3 shows that the proposed approach gives a good agreement for stationary solutions. A difference between the predicted and exact profiles increases for larger S . We find that Eq. (5) gives a reasonable approximation of stationary solutions with vorticity up to $S = 5$.

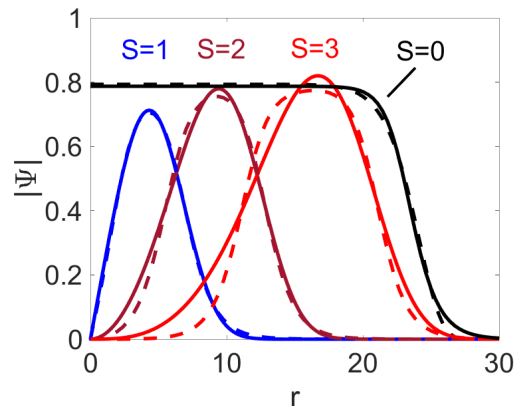


FIG. 3. (color online) Profiles $|\Psi|$ of QDs, found from the VA (solid lines) and from the imaginary-time method (dashed lines) for $S = 0, 1, 2$ and 3 , and $N = 1000, 60, 200$ and 510 , respectively.

According to the Vakhitov-Kolokolov criterion [13], a negative value of the derivative, $d\mu/dN < 0$, means the stability of QDs. Then, as it follows from the inset in Fig. 1, QDs with any S are stable. However this result is valid only for $S = 0$, because the Vakhitov-Kolokolov criterion gives a necessary condition, and it accounts only for the stability along r direction, not on θ . Numerical simulations, using the SSF method, of Eq. (2) up to

$t = 10^4$ show that QDs with $S = 0$ are stable, while vortices with $S > 0$ can be unstable [9]. A typical scenario of an unstable vortex is shown in Fig. 4. As an initial condition of Eq. (2), we use Eq. (5) with stationary parameters, found from the VA. The vortex parameters oscillate slightly, however the vortex form is preserved basically until $t \sim 300$. Then the unstable vortex splits into two QDs with $S = 0$ each. These QDs have both the radial and tangential velocities, however the total momentum is constant (zero). An unstable vortex with vorticity S split typically into $S + 1$ fragments [9].

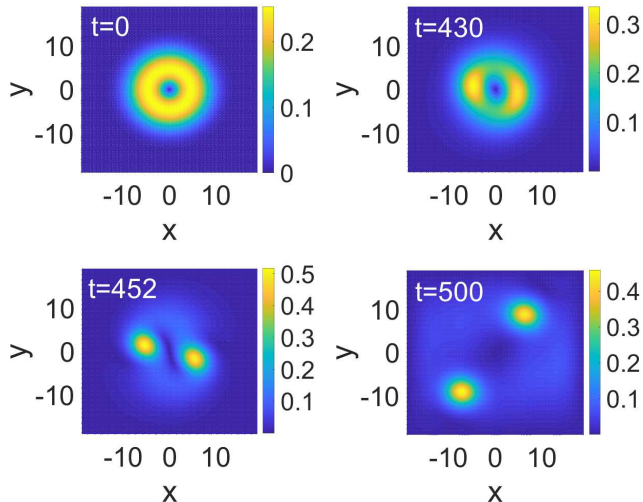


FIG. 4. (color online) The evolution of $|\Psi|$ of the unstable vortex QD for $S = 1$, $N = 10$, $m = 1.232$, $A = 0.082$ ($\bar{A} = 0.253$), and $w = 5.051$.

For a given $0 < S \leq 5$, there is a threshold value N_{th} , below which the vortex is unstable [9]. We confirm this result numerically. For different values of N , we integrate Eq. (2) with initial conditions in a form of Eq. (5) and stationary parameters, found from the VA. We identify a vortex as stable, if there no splitting up to $t \sim 10^4$. We find that for $S = 1, 2$, and 3 , the stability thresholds are $N_{\text{th}} = 60, 200$, and 510 , respectively. This coincide with results of Ref. [9], where it is found also that no stable QDs exist for $S > 5$ and $N \lesssim 10^4$. In Figs. 1 and 2, parameters of unstable QDs are shown by dashed lines.

In Ref. [9], it was stated also that there is another threshold $N_{\text{min}}(S)$ for $0 < S \leq 5$ below which vortices do not exist. In contrast to this work, we find that vortices exist for $N < N_{\text{min}}$ as well, though they are unstable. Initial conditions, found from Eq. (5) with the stationary parameters for $0 < S \leq 5$, remain almost unchanged up to $t \sim 300$ even for small N . This indicates that the initial condition, found from the VA, is close to a stationary (unstable) state. In other words, the initial dynamics of vortices for $N < N_{\text{min}}$ is similar to the dynamics of unstable vortices for $N_{\text{min}} < N < N_{\text{th}}$. For larger t , the vortex splitting occurs, as described above. We mention that the imaginary time method, used in

Ref. [9], requires an additional tuning of parameters for finding *unstable* stationary solutions.

The VA gives also good predictions of the dynamical properties of QDs. Figure 5 illustrates the dependence of the angular frequency Ω_0 of small internal oscillations on N . We use Eq. (5) with slightly (1–5%) perturbed stationary parameters as an initial condition in numerical simulations of Eq. (2). We observe long-lived (up to $t \sim 1000$) oscillations of the QD shape. We measure the period τ from the dependence of $w(t)$ after 4–5 oscillations as an average over 5–10 periods, and the angular frequency is found as $\Omega_0 = 2\pi/\tau$. Figure 5 demonstrates a good agreement for $S = 0$, and a reasonable agreement for $S = 1$.

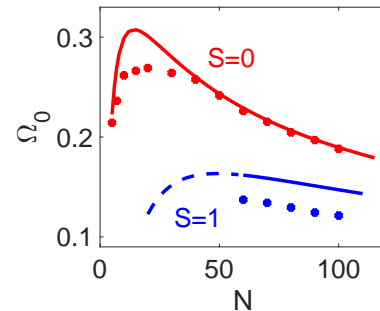


FIG. 5. (color online) The angular frequency Ω_0 of small oscillations of $w(t)$ for $S = 0$ and 1 . Lines are found from Eq. (16), while points are found from numerical simulations. A dashed line corresponds to unstable vortices.

C. Periodic variation of $\delta(t)$

In order to analyze deeper the relevance of the VA, we study the QD dynamics under the action a periodic modulation of parameter $\delta(t)$

$$\delta(t) = \delta_0[1 + \epsilon \sin(\omega_m t)], \quad (19)$$

where ϵ and ω_m are the amplitude and the angular frequency of modulations, respectively. Such modulations can be created by a periodic variation of the external magnetic field via the Feshbach resonance.

The periodic variation of $\delta(t)$ induces oscillations of the QD parameters, such as $A(t)$ and $w(t)$. We analyze the dynamics of the fundamental QD ($S = 0$) for $N = 50$. For given ϵ , the resonance frequency ω_r can be found from the dependence of the amplitude difference $\Delta A \equiv A_{\text{max}} - A_{\text{min}}$ on frequency ω_m , where A_{max} (A_{min}) is the largest (lowest) value of $A(t)$ on time. At $\omega_m = \omega_r$, the amplitude difference has a peak. We find, by solving numerically Eq. (2), that for small ϵ , frequency ω_r is close to the eigenfrequency Ω_0 . Frequency ω_r changes with an increase of ϵ due to nonlinearity.

We consider firstly the QD dynamics for the driving frequency close to $\Omega_0(N = 50) = 0.243$. In Fig. 6a, we

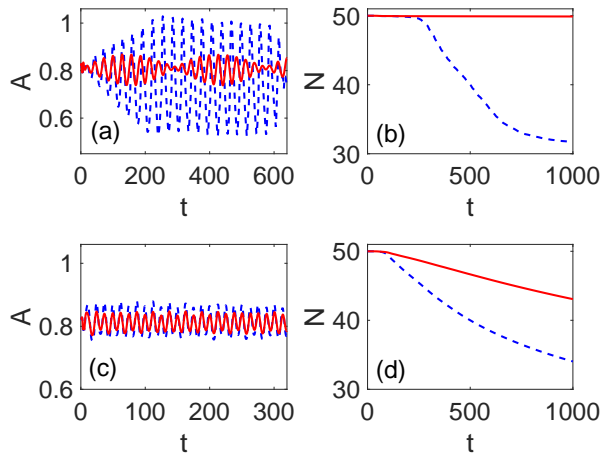


FIG. 6. (color online) The dependencies of amplitude A [(a) and (c)] and norm N [(b) and (d)] on time, found from numerical simulations of Eq. (2) for $\delta_0 = -1$, $S = 0$, and $N = 50$. (a) and (b) $\omega_m = 0.21$, $\epsilon = 0.5\epsilon_1$ (solid lines), and $\epsilon = \epsilon_1$ (dashed lines); (c) and (d) $\omega_m = 0.5$, $\epsilon = 0.5\epsilon_2$ (solid lines), and $\epsilon = \epsilon_2$ (dashed lines), where $\epsilon_1 = 0.187$ and $\epsilon_2 = 0.252$.

plot the dependence of A on t for $\omega_m = 0.21$, $\epsilon = 0.5\epsilon_1$ and $\epsilon = \epsilon_1$, where $\epsilon_1 = 0.187$. A choice of such ω_m and ϵ_1 will be explained below, see also Fig. 7. When $\omega_m = 0.21$ and $\epsilon = 0.5\epsilon_1$, we observe a beating of the QD amplitude, see a solid line in Fig. 6a. This beating is typical for forced oscillations, and it is consistent with the VA approach. Namely, a change of $\delta(t)$ results in a deformation of the potential $U(w)$, see Eq. (12), and a periodic variation of the minimum point. This deformation of $U(w)$ gives rise to oscillations of the QD parameters. Since N almost does not change, see a solid line in Fig. 6b, the dynamics is adiabatic.

An increase of ϵ results usually in oscillations with larger ΔA , as in Fig. 6a for $\omega_m = 0.21$ and $\epsilon = \epsilon_1$ (a dashed line). For these parameters, an increase of the amplitude envelope on time has initially a linear slope that indicates a resonance in oscillations. Oscillations of the QD amplitude result in a strong excitation of the internal mode. The QD starts to emit particles that is observed as round outgoing waves of the BEC density. A dashed line in Fig. 6b shows that the emission of waves begins at $t \approx 200$, and after that N decreases due to the absorbing boundary conditions. Large oscillations result in a QD splitting into two smaller droplets that move in opposite directions. For $\epsilon = \epsilon_1$, the splitting occurs at $t \sim 650$. This type of the dynamics is typical for frequencies $\omega_m \sim \Omega_0$, or for large ϵ . Value ϵ_1 is taken such that N loses 20 % at $t = 500$. We use later a corresponding condition to analyze the dynamics for different ω_m . We mention that splitting of solitons was found also for the nonlinear Schrödinger model with the varying coefficient of the 2BI [14], see also Ref. [15].

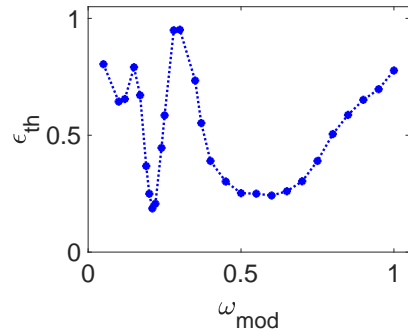


FIG. 7. Threshold ϵ_{th} as a function of ω_m , found from numerical simulations of Eq. (2) for $\delta_0 = -1$, $S = 0$, and $N = 50$.

Now we consider the dynamics out of the resonance for $\omega_m = 0.5$, $\epsilon = 0.5\epsilon_2$ and $\epsilon = \epsilon_2$, where $\epsilon_2 = 0.252$, see Figs. 6c and 6d. After a development of oscillations, see Fig. 6c, the QD emits particles in a form of linear matter waves. This fact follows from a decrease of N starting at $t \sim 100$ in Fig. 6d. The larger values of ϵ induce larger oscillations, and therefore a faster decay of N , see dashed lines for $\epsilon = \epsilon_2$ in Figs. 6c and 6d. Here, ϵ_2 is taken, using the same condition as for ϵ_1 .

For $\epsilon = \epsilon_2$, function $N(t)$ at large t changes very little, and it has some signs of saturation, approaching value $N = 22.3$ at $t = 10^4$. For small ϵ , it takes much longer time to see saturation of $N(t)$, cf. the solid and dashed lines in Fig. 6d. Thus, for small ϵ , we observe that after an emission of an appreciable amount of particles, $N(t)$ changes slowly at large t . This means that a response of a QD to periodic modulations of δ out of the resonance becomes adiabatic at large t . For sufficiently large ϵ , $\epsilon > \epsilon_2$, the asymptotic value of $N(t)$ can be less than 2–5% of its initial value. This corresponds to a substantial evaporation of a QD under the action of periodic modulations.

An analysis of numerical results for different values of ω_m and ϵ reveals four main types of the QD dynamics. In the first type, the QD oscillates adiabatically, with negligible emission of waves. This type occurs for small ϵ . The VA, presented in Sect. II A, is valid for this adiabatic regime. In all of the rest types of the dynamics, the QD emits linear waves after a steady period. This emission of waves corresponds to evaporation of the QD. In the second type of the dynamics, a QD transfers at large t to the adiabatic regime with smaller N . A decrease of N on time changes the parameters of the stationary state, see Fig. 2, and therefore the response to the driving field. In the third type, a QD decays completely via emission of linear waves. For some parameters, this decay takes large time $t > \sim 10^4$. In the fourth type, a QD splits into smaller moving droplets. Since N decreases on time for the last three types of the dynamics, the VA is not applicable for these cases. The first type and the second type are similar, they differ only by the amount

of particles, remaining in the QD. In order to separate the adiabatic regimes (the first and the second types) from the decay and the splitting (the third and the fourth types), we introduce the following criterion. For given ω_m , we find such ϵ_{th} that N decreases at $t = 500$ to 80% from the initial value, and the decrease continues (no saturation), at least, up to $t = 1000$.

The dependence of ϵ_{th} on ω_m is presented in Fig. 7. We can say that ϵ_{th} gives an approximate threshold between different regimes. The adiabatic regimes exist for sure far below the threshold, while the QD splitting or a complete QD decay exist much above this value. There is a narrow minimum near $\omega_m = 0.21$, and a wide deep for $\omega_m = [0.4, 0.7]$. The minimum near $\omega_m = 0.21$ corresponds to resonance oscillations, where the splitting may occur even for small ϵ . We see that the VA gives a proper estimate of the resonance frequency. Curve ϵ_{th} in interval $\omega_m = [0.4, 0.7]$ separates the regime of small and large changes of N .

III. CONCLUSIONS

We have shown, that similarly to the 1D case [12], the super-Gaussian function is a good approximation for 2D quantum droplets. The dynamical equations for the QD parameters have been derived using the VA. Analytical equations for parameters of stationary droplets with

$S = 0$ and $S = 1$ have been obtained. The density of stationary QDs tends to a constant for large N , while the width grows gradually. Such a property characterizes a QD as a cluster of incompressible liquid. Our analysis confirms results of work [9] that QDs with $S = 0$ are stable, while vortices with $0 < S \leq 5$ are unstable, when $N < N_{\text{th}}(S)$.

It was also demonstrated that the VA gives a proper description of the QD dynamics. The frequency Ω_0 of small internal oscillations of QDs has been obtained. Values of Ω_0 gives good (reasonable) approximation for $S = 0$ ($S = 1$). It has been found that modulations of δ with frequency close Ω_0 induces resonance oscillations of the QD parameters. We have identified different regimes of the dynamics, including adiabatic oscillations, the decay of QDs, and the QD splitting, for different parameters of modulations.

The case $\delta > 0$ has been analyzed as well. The VA predicts the existence of stationary vortices, but they are unstable. Vortices either spread dispersively or collapse, depending on a value of the initial width (amplitude).

ACKNOWLEDGEMENTS

This work was supported by grant FA-F2-004 of the Ministry of Innovative Development of the Republic of Uzbekistan.

-
- [1] C. J. Pethick and H. Smith, *Bose-Einstein Condensation in Dilute Gases* (Cambridge University Press, Cambridge, 2008).
 - [2] Ya. V. Kartashov, G. E. Astrakharchik, B. A. Malomed, and L. Torner, *Frontiers in multidimensional self-trapping of nonlinear fields and matter*, *Nature Rev. Phys.* **1**, 185 (2019).
 - [3] D. S. Petrov, *Quantum mechanical stabilization of a collapsing Bose-Bose mixture*, *Phys. Rev. Lett.* **115**, 155302 (2015).
 - [4] D. S. Petrov and G. E. Astrakharchik, *Ultradilute low-dimensional liquids*, *Phys. Rev. Lett.* **117**, 100401 (2016).
 - [5] T. D. Lee, K. Huang, and C. N. Yang, *Eigenvalues and eigenfunctions of a Bose system of hard spheres and its low-temperature properties*, *Phys. Rev.* **106**, 1135 (1957).
 - [6] C. R. Cabrera, L. Tanzi, J. Sanz, B. Naylor, P. Thomas, P. Cheiney, and L. Tarruell, *Quantum liquid droplets in a mixture of Bose-Einstein condensates*, *Science* **359**, 301 (2018).
 - [7] G. Semeghini, G. Ferioli, L. Masi, C. Mazzinghi, L. Wolswijk, F. Minardi, M. Modugno, G. Modugno, M. Inguscio, and M. Fattori, *Self-bound quantum droplets in atomic mixtures*, *Phys. Rev. Lett.* **120**, 235301 (2018).
 - [8] I. Ferrier-Barbut, H. Kadau, M. Schmitt, M. Wenzel, and T. Pfau, *Observation of quantum droplets in a strongly dipolar Bose gas*, *Phys. Rev. Lett.* **116**, 215301 (2016).
 - [9] Y. Li, Z. Chen, Z. Luo, C. Huang, H. Tan, W. Pang, and B. A. Malomed, *Two-dimensional vortex quantum droplets*, *Phys. Rev. A* **98**, 063602 (2018).
 - [10] Ya. V. Kartashov, B. A. Malomed, and L. Torner, *Metastability of quantum droplet clusters*, *Phys. Rev. Lett.* **122**, 193902 (2019).
 - [11] R. Y. Chiao, E. Garmire, and C. H. Townes, *Self-trapping of optical beams*, *Phys. Rev. Lett.* **13**, 479 (1964).
 - [12] Sh. R. Otajonov, E. N. Tsoy, F. Kh. Abdullaev, *Stationary and dynamical properties of one-dimensional quantum droplets*, *Phys. Lett. A* **383**, 125980 (2019).
 - [13] N. G. Vakhitov and A. A. Kolokolov, *Stationary solutions of the wave equation in a medium with nonlinearity saturation*, *Radiophys. Quantum Electron.* **16**, 783 (1973).
 - [14] H. Sakaguchi and B. A. Malomed, *Resonant nonlinearity management for nonlinear Schrödinger solitons*, *Phys. Rev. E* **70**, 066613 (2004).
 - [15] F. Kh. Abdullaev, E. N. Tsoy, B. A. Malomed, R. A. Kraenkel, *Array of Bose-Einstein condensates under time-periodic Feshbach-resonance management*, *Phys. Rev. A* **68**, 053606 (2003).